JOURNAL OF MATERIALS SCIENCE 26 (1991) 1015–1026

Experimental investigation of the effects of stress rate and stress level on fracture in polystyrene

B. L. GREGORY, J. BOTSIS*
Department of Civil Engineering, Mechanics and Metallurgy, University of Illinois at Chicago, Box 4348, Chicago, Illinois 60680, USA

The effects of stress rate and stress level on fatigue crack propagation in compression-moulded single-edge notched specimens (0.25 mm in thickness) of polystyrene are reported. Values of the stress rate $\dot{\sigma}$ are obtained from the formula $\dot{\sigma} = 2\nu(\sigma_{max} - \sigma_{min})$, where ν is the frequency and σ_{max}, σ_{min} are the maximum and minimum stresses of the fatigue cycle. Different levels of $\dot{\sigma}$ are achieved by changing the frequency while keeping σ_{max}, σ_{min} at fixed values. The effect of the stress level is investigated by keeping $\dot{\sigma}$ and σ_{min} constant and varying σ_{max} and ν. The results show that when the kinetic data are plotted as $\Delta l/\Delta t$ against the energy release rate G_1, a relatively small effect of the stress rate is observed. If the same data are treated as $\Delta l/\Delta N$ against G_1, a decrease in $\Delta l/\Delta N$ with test frequency is seen. The increase in the level of σ_{max} results in a higher crack speed. The critical crack length is found to be practically the same for all stress-rate experiments. A decrease in the critical crack length is observed with the increase in stress level. Analysis of craze distribution around the crack path shows that the extent of crazing decreases with the increase in stress rate and increases with the increase in stress level. For all experimental conditions, the ratio of the second moment to the square root of the fourth moment of the histograms of craze density along directions normal to the crack path is found to be constant throughout the slow phase of crack propagation. This result supports a self-similarity hypothesis of damage evolution proposed in the crack layer model.

1. Introduction

Prediction of lifetime of a structure under loads and the characterization of a material's toughness assume a position of prominence in engineering design efforts. Consequently, their understanding and modelling are issues of central importance to engineers and material scientists alike.

In general, engineering materials fail when their load-bearing capacity is compromised by the presence of defects. Upon loading, failure ensues on the microscopic level through the process of damage accumulation which results from the interaction of the pre-existing defects and the applied load. This interaction yields a macroscopic crack (crack initiation) which grows in a stable fashion until dynamic fracture.

Conventionally slow crack propagation as well as criteria for crack instability are described in terms of stress intensity factor K_1, or energy release rate J_1 [1]. However, both K_1 and J_1 are macroscopic parameters. Their use is justified as long as they uniquely characterize the stress and the strain fields in the vicinity of the crack tip. Apparently, K_1 and J_1 do not reflect any fracture process. Thus when the restrictions of "K_1-dominance" or "J_1-dominance" are not met, K_1 and J_1 fail to correlate with the fracture process. Examples are large-scale plasticity, deceleration of a large crack and the behaviour of small cracks. Such discrepancies are attributed to the effect of damage and its interaction with the main crack.

For most engineering materials, a zone of damage accompanies crack propagation under fatigue and creep. Damage nucleation and growth, whether in the form of crazes, microcracks, voids or homogeneous transformations, etc., is a process that absorbs energy; energy that otherwise would be available to drive the crack. Therefore the nature and extent of damage, by and large, determine the useful lifetime and toughness of the material.

Experimental observations on a number of materials have shown that the evolution of a damage zone displays characteristics which are independent of the particular damage elements [2–6]. These observations suggest that a crack and its surrounding damage zone can be treated as a macroscopic entity, a crack layer (CL) [7, 8]. In the CL approach, fracture is modelled as the evolution of the damage zone which surrounds the crack tip. Consequently, four kinematic parameters are introduced to describe a fracture process. The corresponding driving forces are deduced by the use of principles of irreversible thermodynamics. In

* To whom all correspondence should be addressed.

0022–2461/91 $03.00 + .12

this approach, however, the problem of damage evolution is one of critical importance. In addition, formulation of constitutive equations for damage evolution is well recognized by now to be a problem pertinent to a material's fracture. The numerous investigations reported in the literature demonstrate that loading conditions and material morphology assume a pivotal role in the evolution of damage during fracture.

In this first of a two-part series of papers, experimental investigations of the effects of stress rate and stress level on crack growth and craze dissemination in fatigued specimens of polystyrene (PS) are reported. An analysis of the results using the phenomenological model of a CL is presented in a consecutive part.

2. Experimental procedure

2.1. Specimen preparation

Atactic PS used in this study, Styron 685 (M_w = 250 000), was supplied in the form of pellets by Dow Chemical Company. The pellets were washed and dried and then compression-moulded into plaques of 150 mm × 150 mm × 0.25 mm in a Dake press at a platen temperature of 160 °C and a pressure of 7.66 MPa. The plaques were slow-cooled to room temperature in the press. From these plaques, rectangular pieces were cut and machined to the following specimen dimensions: 80 mm in gauge length and 20 mm in thickness. A 60° V-shaped notch was milled into the edge of each test-piece at the mid-span of the gauge length. The machined edges were metallographically polished to a 0.5 μm finish to prevent formation of edge crazes. The polished samples were then annealed at about 10 °C below T_g for 48 h and allowed to cool slowly to room temperature. This treatment is intended to relieve any residual stresses induced during machining and polishing.

2.2. Experimental methods

Tension–tension fatigue experiments were conducted on a dual-actuator servohydraulic Instron materials testing system at ambient temperature in a laboratory atmosphere. All tests were load-controlled with a sinusoidal waveform function.

The stress rate and stress level of each experiment were controlled by making appropriate adjustments in the amplitude and frequency of the loading waveform. Values for the stress rate $\dot{\sigma}$ were calculated from $\dot{\sigma} = 2\nu(\sigma_{max} - \sigma_{min})$. The geometrical interpretation of this relationship in the stress–time plane is shown in Fig. 1.

In the stress level experiments the stress rate, as defined above, and the minimum stress of the fatigue cycle were held constant (at values of 10.50 MPa sec^{-1} and 2.50 MPa, respectively). The frequency was varied (0.35, 0.75, and 2.00 Hz) to achieve maximum stress levels of 17.50, 9.50 and 5.12 MPa, respectively. These values correspond to load ratios R = 0.14, 0.26 and 0.49.

Similarly, in the stress rate experiments the maximum and minimum stresses were held constant (at values of 7.80 and 2.50 MPa) while the frequency was varied (0.33, 1.00, 3.50, 5.00 and 8.00 Hz) to achieve stress rates of 3.50, 10.60, 37.10, 53.00 and 84.80 MPa sec^{-1}, respectively. Obviously, in these experiments the load ratio is the same and equal to R = 0.32.

The stress intensity factor K_1 was calculated according to the formula

$$K_1 = \sigma_{max}(\pi l)^{1/2} f(l/B)$$

Here σ_{max} is the maximum stress of the fatigue cycle, l is the crack length and B is the specimen width. The function $f(l/B)$ is a correction factor related to the specimen geometry [9]. The elastic energy release rate is calculated as $G_1 = K_1^2/E$ where E is the Young's modulus of the material which is evaluated experimentally (E = 4.1 GPa).

Crack growth kinetics and the evolution of the craze zone were observed by means of a Questar long-range travelling microscope, and recorded using a Hamamatsu video system with a recording speed of 30 frames sec^{-1}. Fracture surfaces were examined on a Zeiss universal microscope. Damage analysis was performed on thinned sections prepared according to standard metallographic grinding and polishing techniques [10]. Three specimens were tested at each stress level and stress rate as a check for reproducibility. It was found that the width and length of the active zone as well as the crack growth kinetics and the load at fracture were within experimental error (< 10%).

3. Results

3.1. Macroscopic observations

Fig. 2 exhibits a typical configuration of a crack and the surrounding craze zone in PS investigated in these studies. The system of the crack and the craze zone defines a crack layer (CL) [7, 8]. The active zone is the domain of the CL within which the time rate of craze density is positive; $\dot{\rho} > 0$. The inert zone is the part of the CL complementary to the active zone; $\dot{\rho} = 0$ ($\rho > 0$). The active zone is roughly characterized by the width w and length l_a. The two zones are separated by the trailing edge (Fig. 2).

In the case of a crack cut, the elastic energy release rate G_1, is spent on creating new surfaces. Thus G_1 is the driving force for crack growth. When a crack is surrounded by a zone of damage, G_1 may not be an appropriate parameter to correlate crack propagation data since crazing may significantly alter the stresses and strains around the crack tip. Botsis [11] reports that in commercial PS specimens, values of the energy release rate calculated from load–displacement curves are practically equal to the elastic energy release rate G_1. This is attributed to the small size of the active zone with respect to the crack length and specimen width. The material employed here is compression-moulded and with a Young's modulus almost twice as large as the Young's modulus of commercial PS. In addition, the size of the active zone in both materials is comparable. Therefore we assume that in this case as well, the actual energy release can be approximated by G_1.

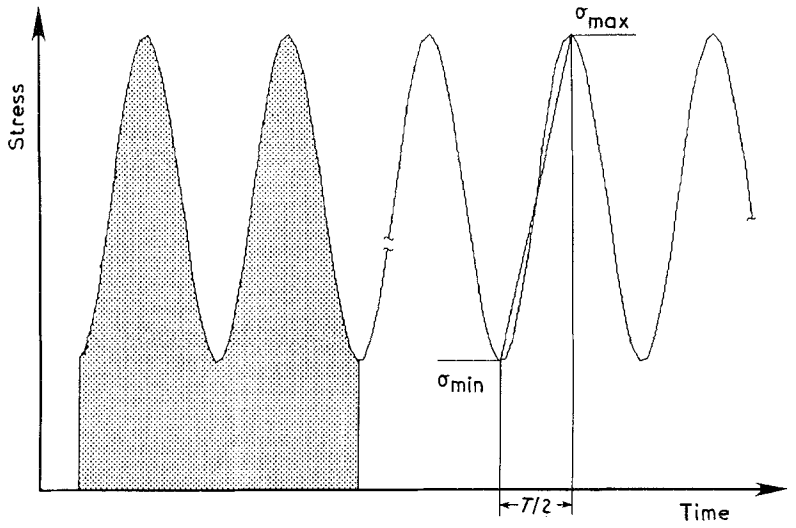

Figure 1 Definition of the stress rate. The shaded area indicates load–time area (see text for details).

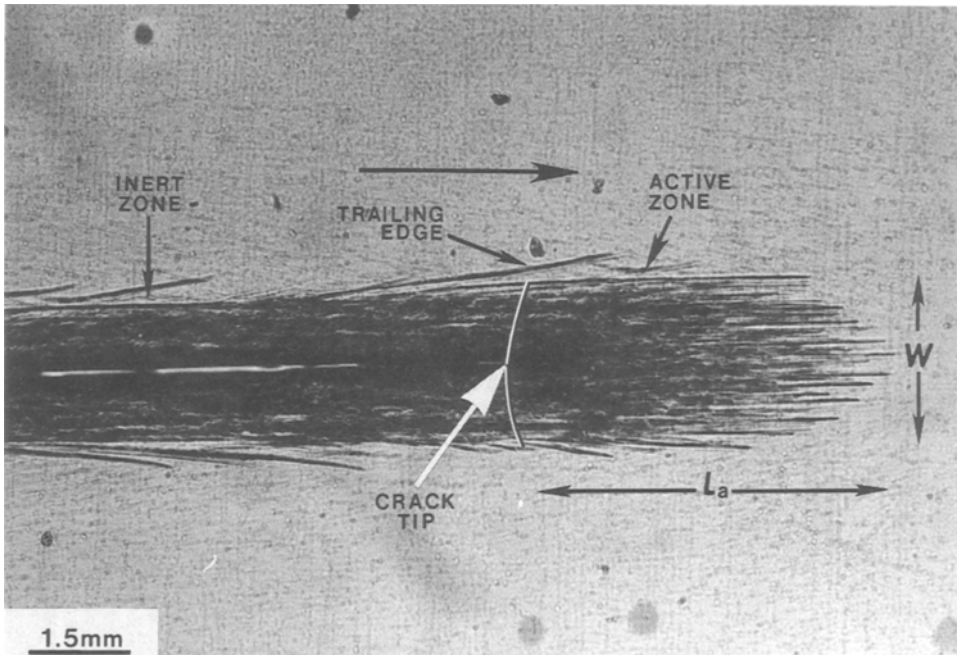

Figure 2 Crack layer configuration in compression-moulded PS.

The evolution of w and l_a with the energy release rate G_1 for both sets of experiments is presented in Figs 3 and 4. Points represent average values of w and l_a which result from three experiments performed at each loading condition. The data show that both w and l_a increase monotonically with the increase in G_1. While the different stress rates do not suggest a trend in w and l_a, the higher stress level results in greater values of w and l_a.

Most of the data on fatigue crack propagation (FCP) reported in the literature are expressed as $\Delta l/\Delta N$, where Δl is the crack length increment that corresponds to the increase in the number of cycles ΔN. Although such a presentation is useful in some cases, the changes in frequency and/or stresses from experiment to experiment makes interpretation of FCP data difficult [12]. To investigate the effects of stress rate and stress level on FCP, we analyse the kinetic data as $\Delta l/\Delta N$ and $\Delta l/\Delta t$ (note that $\Delta l/\Delta t = \nu \Delta l/\Delta N$, where ν is the test frequency).

The crack growth kinetics $\Delta l/\Delta N$, for the range of stress rates investigated here, are shown in Fig. 5a as a function of G_1. The data clearly demonstrate that crack speed decreases substantially with the increase in stress rate (or frequency). A similar effect of the test frequency is reported by Skibo *et al.* [13]. On the other hand, if the same data are plotted as $\Delta l/\Delta t$ against G_1 (Fig. 5b), the effect of stress rate is relatively small throughout the entire range of slow CL propagation. The largest difference is about half an order of magnitude and occurs between the largest and smallest stress rates. A similar trend has been observed in polyurethane elustomer [20].

The effect of stress level on FCP is shown in Fig. 6. In both presentations and for small values of G_1, differences in crack speed are relatively small. For

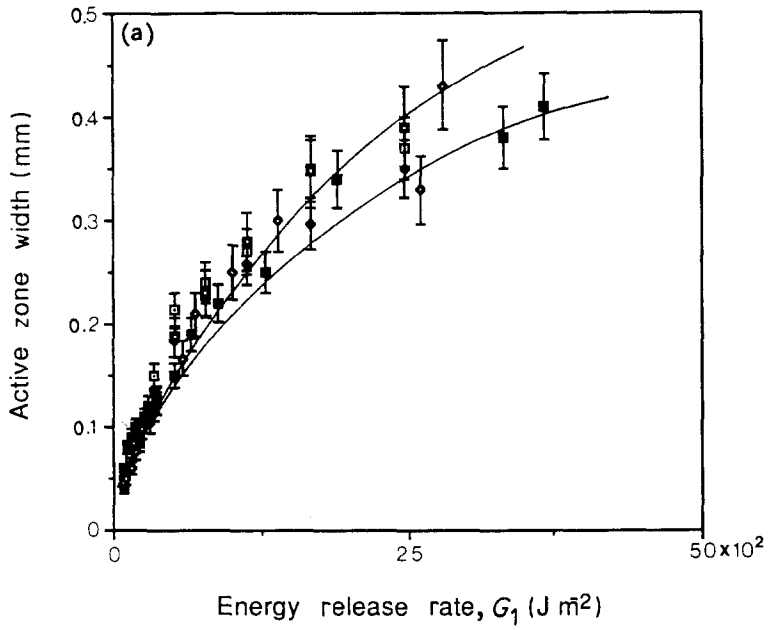

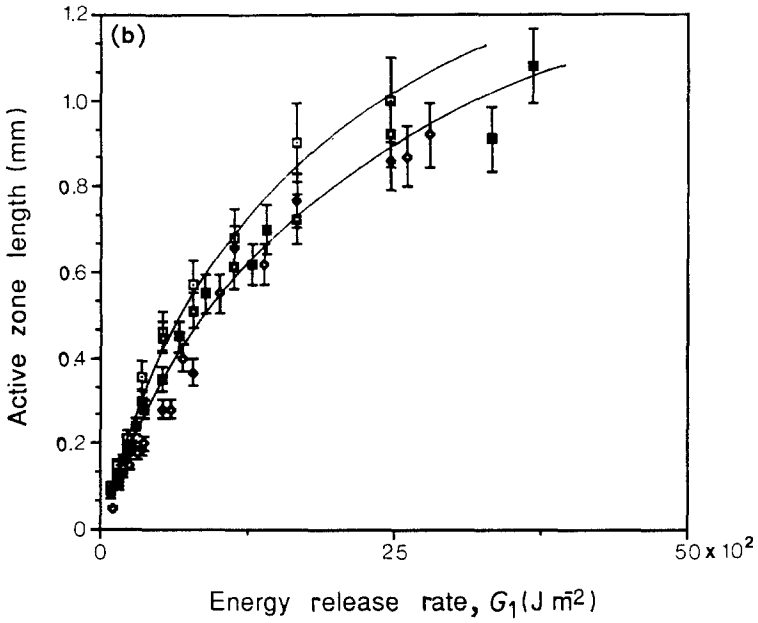

Figure 3 Evolution of (a) w and (b) l_a as a function of G_1 for five different stress rates, $\dot{\sigma}$: (⊡) 3.50, (◆) 10.60, (□) 37.10, (◇) 53.60, (■) 84.80 MPa sec^{-1}.

relatively larger values of G_1 the differences become greater, the tendency being a faster crack speed with an increase in σ_{max}.

3.2. Microscopic observations

Information about the mechanisms of the fracture process is obtained from fracture surface examination and analysis of craze distribution within the damage zone. Optical micrographs of the fracture surface are shown in Fig. 7. During the stable phase of propagation the morphology of the fracture surface appears to be smooth. Striations are observed within the entire range of slow CL propagation (Fig. 7a). In addition, remains of craze material are sporadically seen (arrow A). At the end of the mirror surface, a relatively rough surface is noticed (Fig. 7b). Afterwards, a misty surface is observed which extends up to the edge of the specimen. Similar features are observed in all fractured test-pieces.

Examination of the side view of a CL indicates that the maximum width of the CL corresponds to the end of the smooth surface. It is believed that the change in morphology of the fracture surface which is associated with the maximum width of the CL corresponds to the end of the quasi-static phase of fracture [6]. Thus the end of the mirror-like surface is taken as the end of the stable CL propagation.

Values of the critical crack length l_c for both sets of experiments are shown in Table I. Interestingly, the difference between the highest and the lowest values of l_c is within experimental error for all stress rate experiments investigated in this study. On the other hand, a decrease in the critical crack length is observed with increase in the stress level.

The data in Figs 3 and 4 suggest that the stress rate and stress level have an effect on the extent of crazing during fracture propagation. However, crazing within the damage zone is not uniformly distributed. Therefore to get more insight into the effect of the stress level

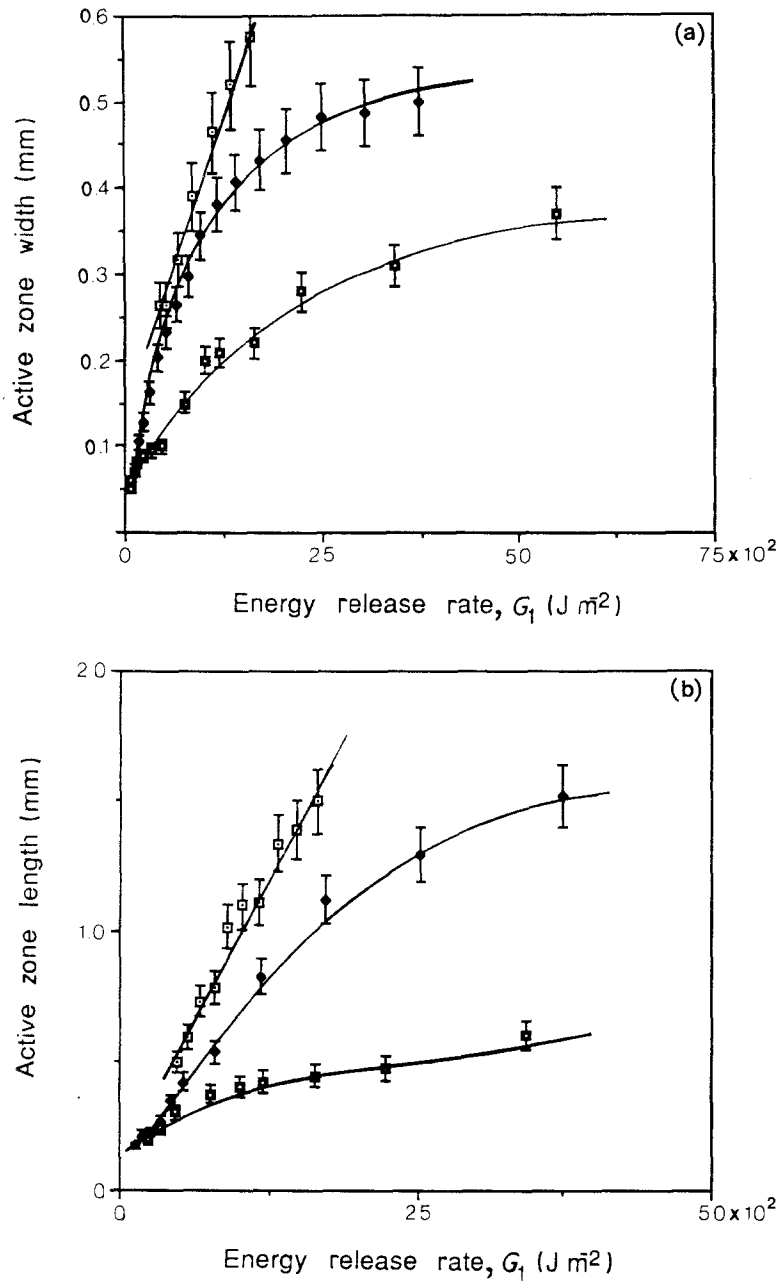

Figure 4 Evolution of (a) w and (b) l_a as a function of G_1 for three levels of σ_{max}: (□) 5.12, (◆) 9.50, (⊡) 17.50 MPa.

and stress rate on the extent of crazing we examined sections normal to the crack propagation direction and parallel to the plane of the specimen.

Fig. 8 displays a transverse section of the lower part of a fractured specimen. Note that crazes are uniformly distributed along the thickness direction, and craze density increases monotonically towards the fracture surface. Thus analysis of craze distribution on sections parallel to the plane of the specimen is sufficient.

Fig. 9 displays parallel sections of the lower half of specimens fractured under the stress rates $\dot{\sigma} = 3.50$, 37.10 and 84.80 MPa sec^{-1} and which correspond to the same level of G_1. Similar sections of the three specimens fatigued under the three stress level are shown in Fig. 10. Interestingly, crazing decreases with the increase in stress rate and increases with the increase in stress level.

From micrographs similar to those displayed in Figs 9 and 10 we constructed histograms of craze density ρ (mm^2 mm^{-3}) [14], along straight lines normal to the crack growth direction. These histograms are compared by examination of the ratio of the second moment μ_2 to the square root of the fourth moment, $(\mu_4)^{1/2}$. The evolution of these ratios is shown in Fig. 11 as a function of the energy release rate G_1. The data suggest that for each experimental condition, $\mu_2/(\mu_4)^{1/2}$ is approximately constant throughout the stable phase of CL propagation. Moreover, it is worth noticing that the ratio is the same for all three stress level experiments.

4. Discussion

The fracture surface morphology shown in Fig. 7 is similar in all test pieces fractured under the various loading conditions investigated in this study. Striations and remains of craze fibrils are observed within the stable phase of CL propagation (Fig. 7a). The smooth, mirror-like appearance suggests that crack growth occurs through a single craze [12]. The change in morphology of the fracture surface at the end of the

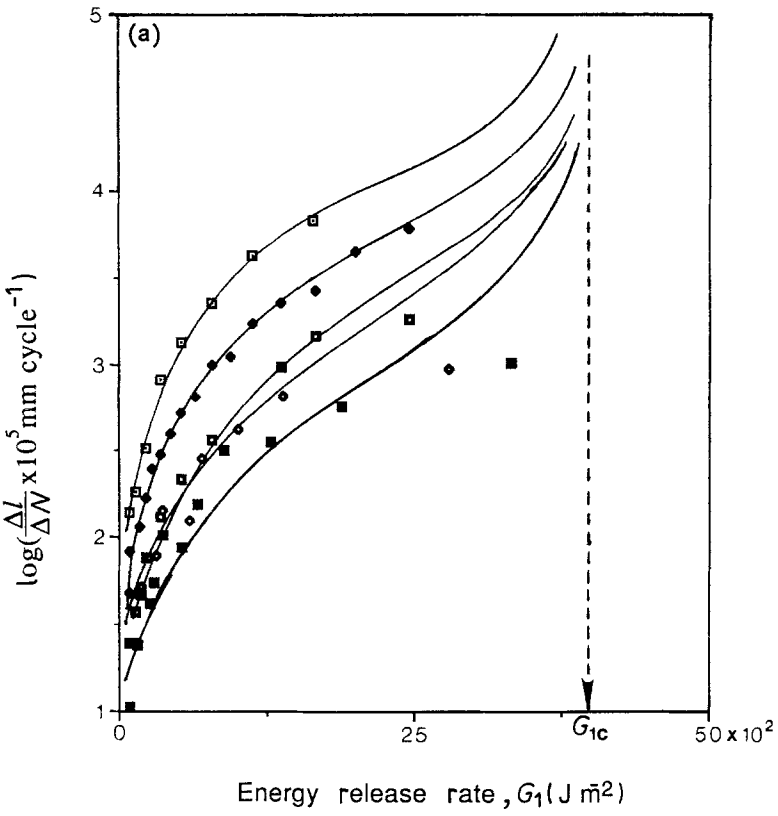

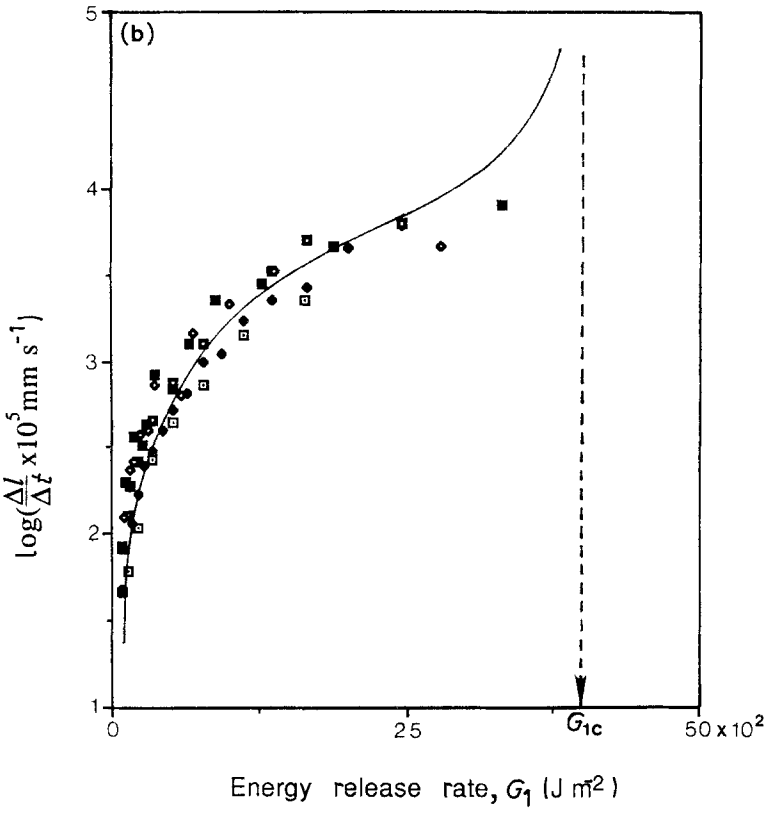

Figure 5 Crack growth kinetics: (a) $\Delta l/\Delta N$ and (b) $\Delta l/\Delta t$, plotted against G_1 for five different stress rates, $\dot{\sigma}$: (⊡) 3.50, (◆) 10.60, (□) 37.10, (◇) 53.60, (■) 84.80 MPa sec^{-1}.

stable propagation (Fig. 7b) indicates that the crack grows through multiple crazes.

The micrographs shown in Fig. 9 suggest that the stress rate has an effect on the craze pattern around the crack path. That is, the higher the stress rate the smaller the extent of crazing. This behaviour may be rationalized in terms of the rate dependence of craze initiation [15, 16]. The fast loading rate suppresses craze initiation which gives rise to a smaller extent of crazing. Moreover, the interaction between the crazes themselves [17] and the crack has an effect on the overall resulting craze pattern. Therefore we may assume that crazing around the crack is dependent on both loading rate and interaction.

The kinetic data presented in Fig. 5b indicate that the effect of the stress rate is relatively small. If the same data, however, are treated as $\Delta l/\Delta N$ against G_1 (Fig. 5a), a significant effect of the test frequency is observed. The data show that the higher the frequency of the fatigue experiment, the slower the crack speed.

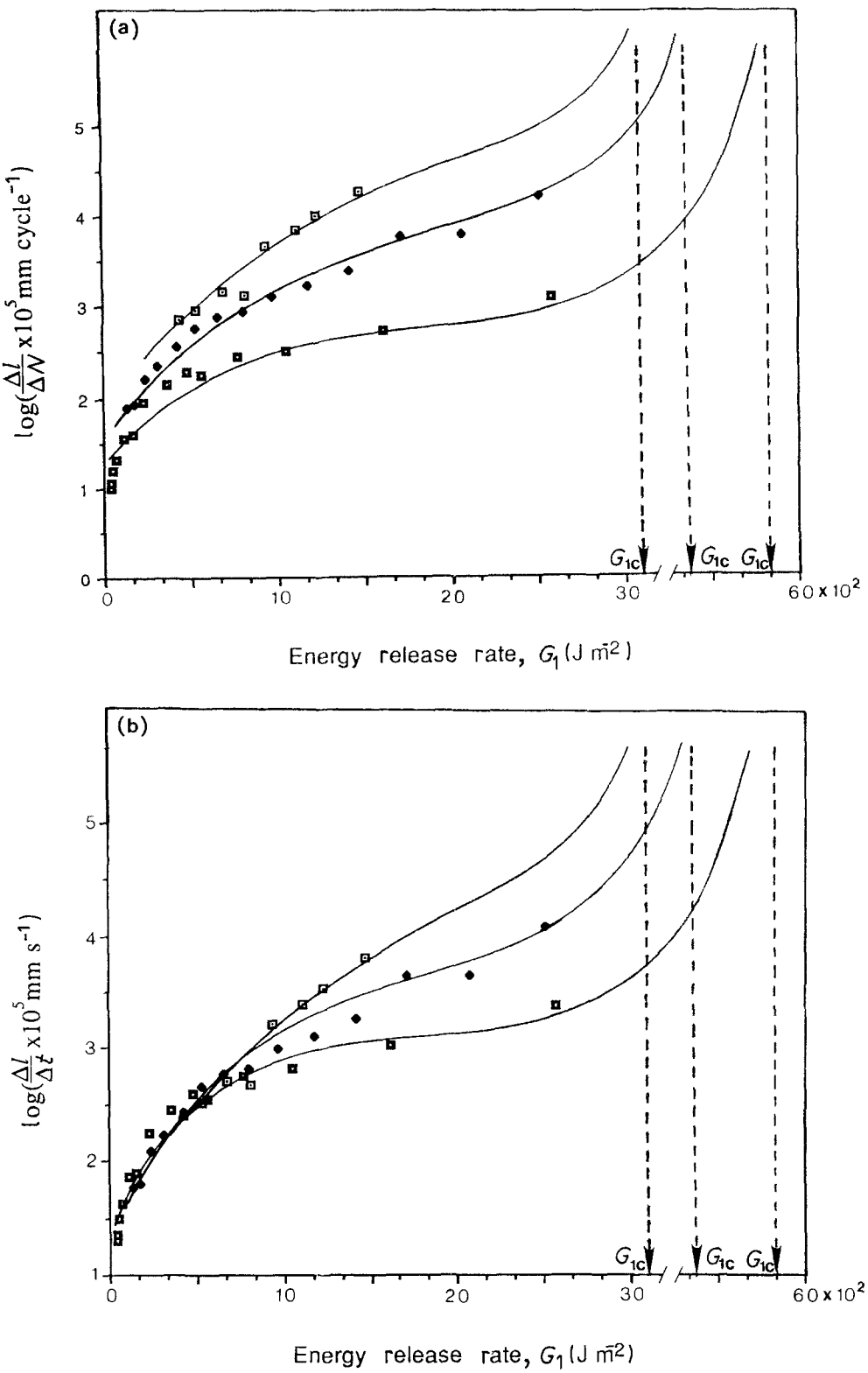

Figure 6 Crack growth kinetics: (a) $\Delta l/\Delta N$ and (b) $\Delta l/\Delta t$, plotted against G_1 for three levels of σ_{max}: (□) 5.12, (◆) 9.50, (⊡) 17.50 MPa.

Notice that for a certain crack growth increment Δl and elapsed time Δt, the corresponding increase in number of cycles is different since $\Delta N = \nu \Delta t$. Accordingly, for the same level of G_1 and different values of frequency ν, the crack speed $\Delta l/\Delta N$ is smaller when $\nu > 1$, or larger when $\nu < 1$, as compared with $\Delta l/\Delta t$.

For the stress rates (or frequencies) employed in this investigation only negligible temperature rise may take place at the crack tip [18]. Hence the observed crack growth behaviour cannot be explained in terms of adiabatic heating effects. The influence of the test frequency on FCP has also been attributed to the strain sensitivity of the modulus. For PS, however, the modulus is practically insensitive to several decades of change in frequency [12]. It is reported [12] that the greatest frequency-sensitivity in polymers which show a high tendency for crazing would be realized when the frequency of the β-transition is comparable to the fatigue test frequency. At room temperature the frequency of β-transition for PS is 10^{-2} Hz. This value is much smaller than the test frequencies employed in the studies reported here.

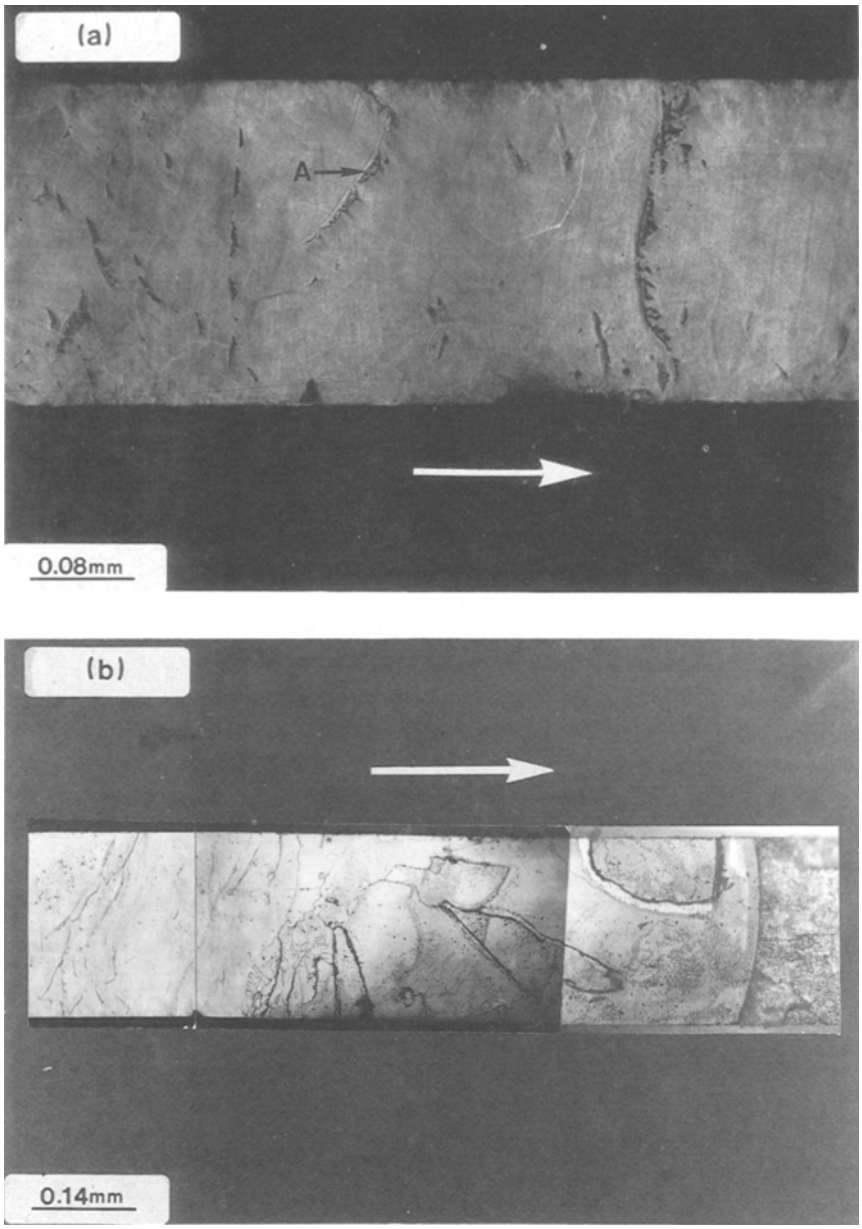

Figure 7 Morphologies of the fracture surface corresponding to (a) slow CL propagation phase, (b) the transition to dynamic fracture. Horizontal arrow indicates the direction of propagation.

TABLE I. Values of critical crack length for different stress rates and stress levels

Frequency (Hz)	Stress rate (MPa sec^{-1})	Critical crack length (mm)
0.33	3.50	9.00
1.00	10.60	9.50
3.50	37.10	10.00
5.00	53.00	9.30
8.00	84.80	9.80
	Stress level (MPa)	
0.35	17.50	5.33
0.75	9.50	9.00
2.00	5.12	12.50

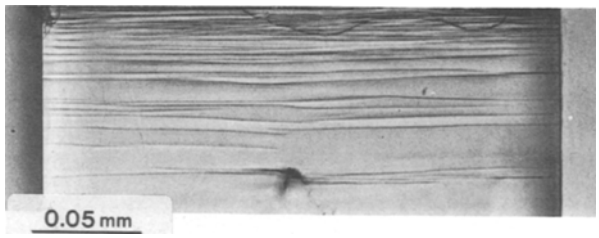

Figure 8 Transverse section of the lower half of a fractured specimen which corresponds to the slow CL propagation.

The effect of frequency on FCP in PS has also been reported elsewhere [12, 13]. It has been shown that increasing the test frequency serves to decrease crack growth rates. The behaviour has been rationalized by the superposition of fatigue and a variable creep component [13].

Crack growth kinetic data reported in the literature are usually presented as $\Delta l/\Delta N$ against the level of stress intensity or energy release rate. Such a presentation, however, renders the comparison of kinetic data difficult when the frequency is changed from experiment to experiment. This is because two variables may contribute to the overall crack propagation behaviour: stress rate (or frequency), and a creep component which results from the different load–time area (LTA) (the latter can be expressed as the area per

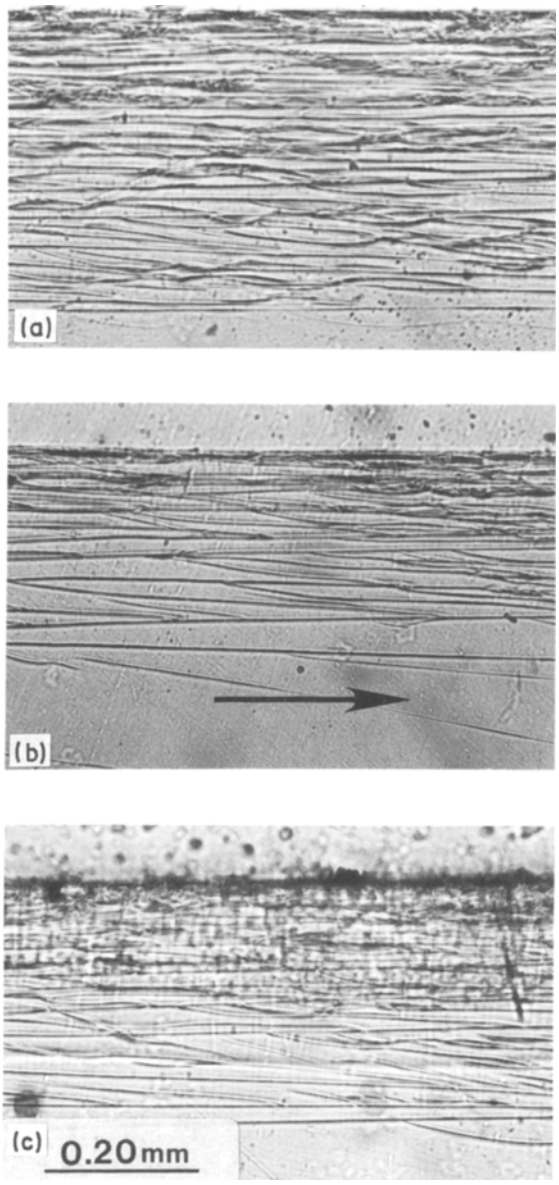

Figure 9 (a–c): lower parts of parallel sections of specimens fractured under three different stress rates and which correspond to $G_1 = 15 \times 10^2\ \mathrm{J\,m^{-2}}$ (see text for details).

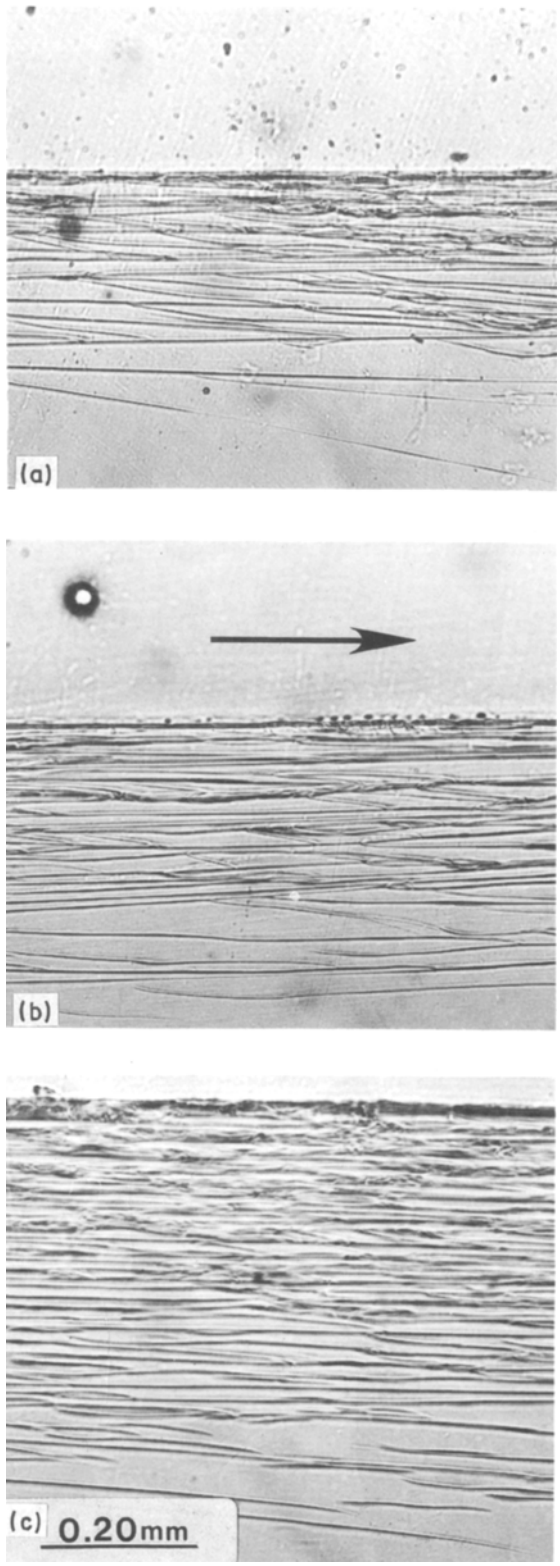

Figure 10 (a–c): lower parts of parallel sections of specimens fractured under three different stress levels and which correspond to $G_1 = 15 \times 10^2\ \mathrm{J\,m^{-2}}$ (see text for details).

cycle or per unit time, under the particular waveform in the stress–time plane, Fig. 1).

To obviate this difficulty, some investigators have examined the effect of loading rate on FCP in polymers by conducting experiments at a certain frequency but with different waveforms [12]. Although an effect of load waveform on crack growth rate is observed, the different waveforms give rise to different values of LTA per cycle, thus making it difficult to isolate the two effects.

The preceding discussion demonstrates that if different frequencies and the same waveform are employed, the LTA per cycle and load rate cannot be isolated. On the other hand, in all stress rate experiments the stress amplitude and mean stress level are kept constant (Section 2.2). Accordingly, when the kinetic data are treated as $\Delta l/\Delta t$, the following argument applies. The LTA per second is the same in all experiments when Δt is a multiple of the cyclic period T, of the experiment with the smallest frequency ($\nu = 0.33$ Hz, $T \approx 3$ sec). When Δt is not a multiple of T the differences in LTA $\mathrm{sec^{-1}}$, from experiment to experiment, are negligibly small when measurements are made over several seconds. This is the case when the average crack speed is low. In the present studies these differences are expectedly small. Differences in LTA $\mathrm{sec^{-1}}$ would become relatively large shortly before specimen fracture (last one or two measurements)

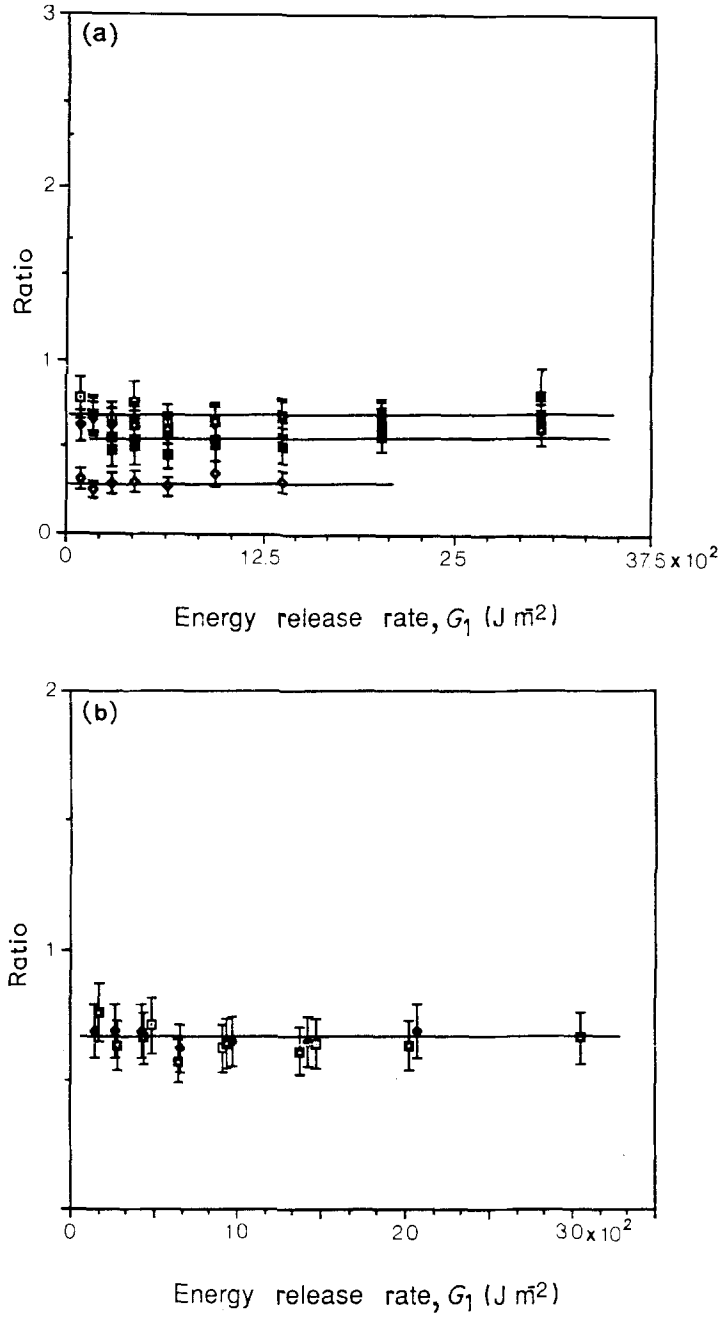

Figure 11 Evolution of ratios $\mu_2/(\mu_4)^{1/2}$. (a) For different stress rates, $\dot{\sigma}$: (⊡) 3.50, (◆) 10.60, (□) 37.10, (◇) 53.00, (■) 84.80 MPa sec^{-1}. (b) For different stress levels, σ_{max}: (□) 5.12, (◆) 9.50, (⊡) 17.50 MPa.

because the average crack speed is high and measurements may be made at time intervals shorter that T (Note that the magnitude of the differences depends upon the frequencies used). This problem can be avoided if fracture surfaces display clear striations and crack growth occurs with every cycle prior to specimen fracture. Accordingly, the last points of crack propagation could be obtained from fracture surfaces so that Δt is a multiple of T. If this is not the case, evaluation of LTA sec^{-1} for every experiment requires accurate crack growth measurements. However, this is experimentally difficult to obtain with conventional optical techniques. Although, fracture surfaces of the material used in these studies (Fig. 7a) display striations, it was difficult to establish a correspondence between striations and number of cycles. Thus, with the exception of the last one to two points, which may not have comparable LTA sec^{-1}, crack propagation behaviour shown in Fig. 5b is assumed to be the result from variations in stress rate only.

The data in Fig. 5 indicate that while the stress rates 3.50, 10.60 and 37.10 MPa sec^{-1} have a negligible effect on crack growth kinetics, a tendency to higher kinetics is observed for the stress rates 53.00 and 84.80 MPa sec^{-1}. The largest difference is less than half an order of magnitude, and is observed between the smallest and greatest stress rate.

The micrographs of Fig. 9 show that the smaller the stress rate the larger the amount of crazing around the crack path. Therefore one would expect higher kinetics with the increase in the stress rate, since more energy is spent on damage formation and growth and less on crack propagation. Although this seems to be the case for $\dot{\sigma}$ = 53.00 and 84.80 MPa sec^{-1}, the differences in kinetics observed under the stress rates of 3.50, 10.60 and 37.10 MPa sec^{-1} are negligible. This may be due to the fact that craze nucleation and growth are relatively low-energy processes. Consequently, it is difficult to record changes in the total potential energy of the specimen caused by craze

nucleation and growth through mechanical experiments. Therefore, in spite of the different amounts of damage observed, its effect on crack speed is not seen.

In the different stress level experiments we changed the levels of σ_{max} while keeping $\dot{\sigma}$ and σ_{min} of the fatigue cycle the same. These experimental conditions are achieved by employing different frequencies in each experiment (Section 2.2). That is, we could not investigate the effect of a load level having the same load rate without changing the frequency. The range of frequencies employed in the load level experiments, however, have a negligible effect on crack propagation when the data are treated as $\Delta l/\Delta t$ (Fig. 5b). Accordingly, we assume that the effect of test frequency and any possible cross-effects resulting from changes of σ_{max} and frequency are negligible in the data shown in Fig. 6b.

The kinetics of crack growth for the different stress level and same stress rate experiments are plotted in Fig. 6b as $\Delta l/\Delta t$ against G_1. Here, the change in σ_{max} results in different values of LTA sec^{-1} from experiment to experiment, the tendency being a larger LTA sec^{-1} with the increase in σ_{max}. Furthermore, it is not possible to isolate the effect of stress level and LTA sec^{-1} when the stress rate is kept constant. Hence the behaviour of crack growth (Fig. 6b) may be due to both stress level and LTA sec^{-1}. Note that the same arguments apply when the data are treated as $\Delta l/\Delta N$ against G_1.

The micrographs of Fig. 10 indicate that the greater the stress level, the larger the extent of crazing around the crack path. If the energy spent for damage controls crack growth, larger damage zones would result in a lower FCP. The crack growth kinetics, however, show an opposite trend (Fig. 7).

When a crack is surrounded by a zone of crazes, the energy release rate G_1, is distributed between the crack itself and the damage [19]. The relative distribution depends upon the specific energy for craze formation, the amount of crazing and its effect on the crack tip stress. The extent to which crack–craze interaction and amount of crazing contribute to fracture behaviour of the material reported herein is a function of craze distribution, their length and opening at various stages of their development. It is difficult, however, to assess their contribution with the available experimental and analytical techniques. Answers to these questions should await the development of more refined analytical methods and improved experimental techniques.

The data in Fig. 11 suggest that for each loading condition the ratio $\mu_2/(\mu_4)^{1/2}$ remains constant throughout the slow CL propagation. These findings are in favour of a self-similarity hypothesis of damage evolution adopted in the phenomenological model of a CL [7, 8]. It is also worth noticing that $\mu_2/(\mu_4)^{1/2}$ is independent of the stress level (Fig. 11b). These results may be looked upon as a similitude criterion for the particular fracture process reported in this paper.

The values of the critical crack length l_c shown in Table I indicate that whereas l_c decreases with the increase in σ_{max}, the effect of stress rate, or for that matter the effect of test frequency, on l_c is within experimental error. In the latter case one would expect different values of l_c, since the different load rate histories result in different amounts of crazes (Fig. 9). However, craze nucleation and growth are relatively low-energy processes. Thus it is difficult to record changes in the total energy caused by nucleation and growth of crazes at global instability. Consequently, at critical propagation the available energy for fracture is seemingly expended on crack growth. This resembles a Griffith-type instability, which implies that the applied stress (σ_{max} of the fatigue cycle) and crack length play the dominant role at the transition to dynamic fracture.

5. Conclusions

The effect of stress rate on FCP has been investigated by conducting experiments with different frequencies and with constant stress amplitude and mean stress level. These experimental conditions allow for the isolation of rate and creep contributions if the kinetic data are treated as $\Delta l/\Delta t$ against the energy release rate G_1.

The experimental results reported in this paper have shown the following:

1. A relatively small effect of the stress rate on FCP is observed when kinetic data are treated as $\Delta l/\Delta t$ against G_1 (Fig. 5). When we account for the different frequencies employed in each experiment (i.e. plotting the data as $\Delta l/\Delta N$ against G_1), a decrease in crack growth kinetics is seen with an increase in test frequency.
2. An increase in crack growth kinetics results from the increase in stress level.
3. The extent of crazing around the crack path is found to increase with the increase in stress level and decrease with increases in stress rate $\dot{\sigma}$.
4. The critical crack length l_c is found to decrease with the increase in the stress level and to be practically independent of the stress rates investigated here.
5. Fracture surface morphology appears to be similar for all experimental conditions, and indicates that fracture propagates through a single craze.
6. Craze distributions along directions normal to the crack path are related by a scalar parameter.

Acknowledgements

The authors wish to acknowledge financial support from the AFOSR underground 89-0505, and thank Dr Clive P. Bosnyak of Dow Chemicals for supplying the Styron 685.

References

1. K. HELLAN, "Introduction to Fracture Mechanics" (McGraw-Hill, New York, 1984).
2. A. CHUDNOVSKY and M. BESSENDORF, "Crack Layer Morphology and Toughness Characterization in Steels", NASA Report 168154 (1983).
3. A. CHUDNOVSKY, A. MOET, R. J. BANKERT and T. M. TAKEMORI, *J. Appl. Phys.* **54** (1985) 5562.
4. N. HADDAOUI, A. CHUDNOVSKY and A. MOET, *Polymer* **27** (1985) 1377.

5. P. X. NGUYEN and A. MOET, *J. Vinyl Tech.* **7** (1985) 140.
6. J. BOTSIS, A. CHUDNOVSKY and A. MOET, *Int. J. Fract.* **33** (1987) 263.
7. A. CHUDNOVSKY, "Crack Layer Theory", NASA Report 174636 (1984).
8. *Idem*, in Proceedings of 10th US National Conference on Applied Mechanics, edited by J. P. Lamb (ASME, Austin, Texas, 1986) p. 97.
9. H. TADA, P. C. PARIS and G. P. IRWIN, "The Stress Analysis of Cracks Handbook" (Del Research Corp., Helertown, Pennsylvania, 1975).
10. A. S. HOLIK, R. P. KAMBOUR, D. G. FINK and S. Y. HOBBS, "Microstructural Science", edited by LeMay, Fallon and McCalls, Vol. 7 (Elsevier-North Holland, 1979) p. 357.
11. J. BOTSIS, *Polymer* **29** (1988) 457.
12. R. W. HERTZBERG and J. A. MANSON, "Fatigue in Engineering Plastics" (Academic, New York, 1980).
13. M. D. SKIBO, R. W. HERTZBERG and J. A. MANSON, *J. Mater. Sci.* **11** (1976) 479.
14. J. BOTSIS, *ibid.* **24** (1989) 2018.
15. A. S. ARGON and J. G. HANNOOSH, *Phil. Mag.* **5** (1977) 1195.
16. B. KOLTISKO, N. BALASHIN, A. HILTNER and E. BAER, in Proceedings of 29th Conference, Society of Plastics Engineers–ANTEC, Chicago, 1983 p. 325.
17. O. J. McGAREL and R. P. WOOL, *J. Polym. Sci.* **B25** (1987) 2541.
18. J. A. SAUER and G. C. RICHARDSON, *Int. J. Fract.* **16** (1980) 499.
19. A. CHUDNOVSKY and SHAUFU WU, *ibid.* **44** (1990) 43.
20. W. G. KNAUSS, in "Advances in Fracture Research ICF7", edited by K. Salama, K. Ravi-Chandar, D. N. R. Taplin and P. Rama Rao, Pergamon Press, NY, Vol. 4 (1989) p. 2683.

Received 2 February
and accepted 19 February 1990